Journal of Catalysis 273 (2010) 9–17

Contents lists available at ScienceDirect

Journal of Catalysis

journal homepage: www.elsevier.com/locate/jcat

Cobalt species and cobalt-support interaction in glow discharge plasma-assisted Fischer–Tropsch catalysts

Jingping Hong [a,b], Wei Chu [b,*], Petr A. Chernavskii [c], Andrei Y. Khodakov [a,**]

[a] Unité de Catalyse et de Chimie du Solide, UMR 8181 CNRS, Bât. C3, USTL-ENSCL-EC Lille, Cite Scientifique, 59655 Villeneuve d'Ascq, France
[b] Department of Chemical Engineering, Sichuan University, Chengdu 610065, China
[c] Department of Chemistry, Moscow State University, 119992 Moscow, Russia

ARTICLE INFO

Article history:
Received 26 February 2010
Accepted 20 April 2010
Available online 23 May 2010

Keywords:
Clean fuels
Fischer–Tropsch synthesis
Cobalt catalyst
Dispersion
Reducibility
Cobalt–silica interaction
Glow discharge plasma
Ruthenium promotion

ABSTRACT

Cobalt species and cobalt-support interaction in glow discharge plasma-assisted Fischer–Tropsch catalysts were studied using a combination of characterization techniques (X-ray diffraction, thermo-gravimetric analysis, temperature-programmed reduction, *in situ* magnetic measurements and *in situ* X-ray absorption). The catalysts were prepared by incipient impregnation using solutions of cobalt nitrate and ruthenium nitrosyl nitrate followed by plasma or/and oxidative treatment.

Cobalt dispersion in silica-supported catalysts was significantly enhanced by plasma pretreatment. Cobalt particle size was a function of glow discharge plasma intensity. The concentration of cobalt silicate in plasma-assisted samples was low. No noticeable effect of the plasma pretreatment on the formation of barely reducible cobalt silicate species was observed. Cobalt reducibility was to some extent hindered in the plasma-assisted catalysts, while promotion with ruthenium significantly enhanced cobalt reducibility in silica-supported catalysts. Due to the combination of high cobalt dispersion and optimized cobalt reducibility, ruthenium-promoted plasma-assisted cobalt catalyst exhibited an enhanced activity in Fischer–Tropsch synthesis.

1. Introduction

Fischer–Tropsch (FT) synthesis converts natural gas-, coal- and biomass-derived syngas into liquid fuels which are totally free of sulfur- and nitrogen-containing compounds and have very low aromatic contents. The interest in FT synthesis has been due to the shortage of petroleum crude oil reserves and environmental constraints [1–3]. Cobalt-based catalysts could be the catalysts of choice for low-temperature FT synthesis [1–3]: they have high activity, high selectivity to linear C_{5+} hydrocarbons, low activities for water–gas shift reaction, and lower price compared to noble metals.

FT synthesis proceeds on cobalt metal sites. The overall number of cobalt sites on supported catalysts depends on both cobalt dispersion and reducibility. In monometallic cobalt catalysts, however, an increase in cobalt dispersion often coincides with a drop in cobalt reducibility [2–6]. Indeed, smaller cobalt particles are usually more difficult to reduce than larger ones. In addition, very small cobalt particles in highly dispersed catalysts could strongly interact with support. This leads to the formation of mixed oxides (i.e., cobalt silicates in the case of Co/SiO_2 catalysts), which are difficult to reduce and which are inactive for FT synthesis [6]. Use of catalyst promoters such as noble metals can break this dispersion-reducibility dependence. In addition to the overall number of cobalt surface sites, the catalytic performance of cobalt-based FT catalysts can be affected by cobalt particle size [7–14]. Cobalt particles with the optimal size (6–10 nm), higher reducibility and higher stability are required for the design of efficient cobalt FT catalysts [2,3,8,11].

Plasma is an ionized gas that can be generated by a number of methods, including electric discharges (glow, microwave, plasma jet, radio frequency). Glow discharge plasma is a kind of non-thermal plasma, which is characterized by high electron temperature (10,000–100,000 K) and relatively low gas temperature [15]. Plasma intensity is determined by the applied power in terms of electric voltage and gap between two electrodes. The energetic species (electrons, ions and radicals) in the plasma could modify the catalyst surface, particle size and morphology of active phase, as well as active phase-support interactions in the catalysts [16]. Catalyst pretreatment with plasma could lead to some specific catalytic properties [15–22]. Various catalysts such as Pd/HZSM [17,19], Pt/NaZSM-5 [21], Ni-Fe/Al_2O_3 [20], Pt/TiO_2 [22] and Pd/Al_2O_3 [23] were treated by glow discharge plasma and tested in different

* Corresponding author.
** Corresponding author. Fax: +33 3 20 43 65 61.
E-mail addresses: Chuwei1965@scu.edu.cn (W. Chu), Andrei.khodakov@univ-lille1.fr, andrei.khodakov@ec-lille.fr (A.Y. Khodakov).

0021-9517/$ - see front matter © 2010 Elsevier Inc. All rights reserved.
doi:10.1016/j.jcat.2010.04.015

catalytic processes, including methane combustion [17,19], NO reduction by methane [21], partial oxidation of methane [20,24] and others.

The plasma technique has not been well explored for the design of cobalt catalysts for FT synthesis. Chu et al. [25] have recently investigated the effects of pretreatment with glow discharge plasma on cobalt dispersion, reducibility and catalytic performance in alumina-supported catalysts in FT synthesis and gained some preliminary results. No information about the influence of glow discharge plasma on metal dispersion and catalytic performance of silica-supported cobalt FT catalysts has been available in the literature.

In this work, a series of silica-supported cobalt-based catalysts were prepared by glow discharge plasma with different plasma power voltages (which correspond to different plasma intensities). The effects of pretreatment with glow discharge plasma on cobalt dispersion, reducibility and structure of monometallic and bimetallic silica-supported cobalt FT catalysts were investigated using a wide range of methods, including X-ray diffraction (XRD), temperature-programmed reduction (TPR), *in situ* and *ex situ* X-ray absorption spectroscopy (XANES and EXAFS), propene chemisorption and *in situ* magnetic method. The catalytic performance in FT synthesis was evaluated in a fixed-bed microreactor.

2. Experimental

2.1. Catalyst preparation

The silica-supported cobalt catalysts were prepared by conventional incipient wetness impregnation of silica gel using aqueous solutions of cobalt nitrate; for the catalysts promoted with Ru, the impregnating solution also contained ruthenium nitrosyl nitrate. A commercial silica gel (Qingdao Haiyang Chemical Co., Ltd., China), with S_{BET} = 355 m^2/g, pore diameter of 7.8 nm, and total pore volume of 0.90 cm^3/g, was used as a catalytic support. After impregnation, the catalysts were dried at 363 K in an oven for 10 h.

The samples after impregnation and drying were divided into two parts. One part was heated in air flow at 523 K for 5 h to obtain conventionally calcined cobalt catalysts; the temperature ramping was 2.5 K/min. Co/SiO_2 and $CoRu/SiO_2$ labels correspond to the conventional catalysts which were prepared without plasma (Table 1). To obtain the plasma-assisted cobalt catalysts, the impregnated and dried samples were first evacuated in the apparatus shown in Fig. 1. Then, they were exposed in the same setup to glow discharge nitrogen plasma for 60 min and then to hydrogen plasma for another 60 min (power voltage = 60–120 V, frequency = 13.56 MHz, initial gas pressure 50 Pa). The quartz tube (Fig. 1) was slowly rotating during the pretreatment to ensure uniform exposure of the catalyst powder to the glow discharge. After the plasma pretreatment, the cobalt catalysts were further calcined in a flow of air at 523 K for 5 h. The monometallic and ruthenium-promoted bimetallic cobalt-based catalysts are designated "Co/SiO_2-P voltage" and "$CoRu/SiO_2$-P voltage", respectively, where "Ru" indicates ruthenium promotion and "P voltage" indicates the voltage used in the glow discharge plasma pretreatment. Before the reaction, all the catalysts were reduced in a flow of hydrogen at 673 K for 5 h. The temperature ramping rate was 3 K/min.

Table 1
Silica-supported cobalt catalysts.

Catalyst symbol	Co content (wt.%)	Ru content (wt.%)	Glow discharge voltage (V)	Co_3O_4 particle size (nm) XRD	Propene chemisorption (10^{-6} mol/g-catal.)
Co/SiO_2	10	–	–	10.2	16.0
Co/SiO_2-P60	10	–	60	8.5	24.2
Co/SiO_2-P80	10	–	80	6.8	–
Co/SiO_2-P100	10	–	100	6.0	–
Co/SiO_2-P120	10	–	120	5.7	13.4
$CoRu/SiO_2$	10	0.3	–	9.8	27.1
$CoRu/SiO_2$-P60	10	0.3	60	5.8	32.1

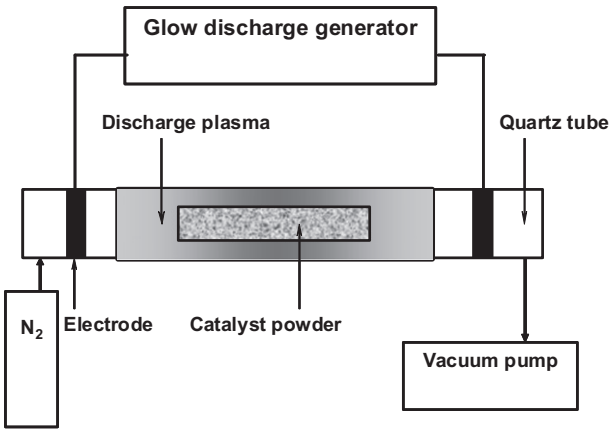

Fig. 1. Schematic of the apparatus for catalyst pretreatment with glow discharge plasma.

2.2. Thermo-gravimetric analysis

Thermo-gravimetric analysis (TGA) was carried out in a flow of air at a heating rate of 5 K/min with a DSC-TGA SDT 2960 thermal analyzer. The sample loading was typically 16 mg.

2.3. Conventional and synchrotron-based X-ray diffraction

Conventional X-ray powder diffraction patterns were recorded at ambient conditions with Cu (Kα) radiation using a Siemens D5000 diffractometer. The average Co_3O_4 crystallite size was calculated from 511 ($2\theta = 59.58^\circ$) diffraction lines according to the Scherrer equation [26].

In situ synchrotron-based XRD patterns were measured at BM01B (SNBL) beamline (ESRF, Grenoble, France). The synchrotron beam wavelength (λ) was set to 0.5 Å. The samples were loaded in quartz capillaries and reduced in hydrogen at 623 K (temperature ramp 3 K/min). The XRD patterns were recorded *in situ* in hydrogen flow at 623 K.

2.4. Temperature-programmed reduction

The temperature-programmed reduction profiles were obtained by passing 5% H_2/Ar gas mixture through the catalyst while increasing the temperature at a linear rate using a Micromeritics AutoChem II Automated Catalyst Characterization System. The sample amount for the experiments was about 50 mg. The gas flow velocity was 30 cm^3/min, and the rate of temperature ramping was 3 K/min.

2.5. In situ magnetic measurements

In situ magnetic measurements were performed using a Foner vibrating-sample magnetometer as described previously [27,28]. The design of the magnetometer allows recording curves of magnetization during temperature-programmed heating or under isothermal conditions at 282–973 K. The catalyst is loaded in a continuous-flow

quartz microreactor equipped with a built-in Pt–PtRh thermocouple. The experiments were conducted by passing pure H_2 through the catalyst while increasing the temperature at a linear rate. The amount of samples for all measurements was around 20 mg. The catalyst was reduced in hydrogen; the temperature increased from 293 to 773 K and then it was kept constant at 773 K. The appearance of metallic cobalt species in the samples was monitored *in situ* by a continuous increase in magnetization during the reduction [27,28].

2.6. Ex situ and in situ X-ray absorption measurements

The X-ray absorption fine structure (XAFS) spectroscopy at the Co K-edge was measured at the BL11.1 beamline in Elettra Synchrotron Light Laboratory, Trieste (Italy). Both *ex situ* characterization of calcined catalysts and *in situ* reduction in hydrogen were performed using our homemade X-ray absorption cell [29]. The measurements were performed in transmission mode, with two ionization chambers used for X-ray detection. The Si (1 1 1) double-crystal monochromator was calibrated by setting the first inflection point of the K-edge spectrum of Co foil at 7709 eV. Measuring an X-ray absorption spectrum (7400–8700 eV) took about 30–40 min. The X-ray absorption data were analyzed using the IFEFFIT procedure. The XANES spectra after background correction were normalized by the edge height. After subtracting cobalt atomic absorption, the extracted EXAFS signal was transformed without phase correction from *k* space to *r* space to obtain the radial distribution function (RDF). Crystalline Co_3O_4, CoO, cobalt nitrate, cobalt foil and α-cobalt silicate were used as reference compounds for XANES and EXAFS analysis. The characteristic XANES spectra and EXAFS Fourier transform moduli of the reference compounds are available from our previous publications [4,30].

2.7. Propene chemisorption

The number of surface metal sites in the catalysts was evaluated by propene chemisorption in a pulse reactor [31]. After reduction in pure hydrogen at 673 K, using the same procedure as for catalytic measurements, the catalyst sample (0.2 g + 0.2 g SiC) was cooled and purged with He at 323 K. Pulses of propene (0.25 cm^3) were introduced into the flow of He. The relative number of metal surface sites was estimated from the amount of chemisorbed propene. No propene chemisorption was observed on pure silica support. Analysis of the reaction products was performed using gas chromatography with a packed column containing XOA 400 silica. The pulse experiments were completed when the detector showed no propene chemisorption. Note that no assumption was made about the stoichiometry of propene chemisorption, this method provides only relative information about the concentration of cobalt metal sites in different catalysts.

2.8. Catalytic measurements

The FT catalytic measurements were carried out in a fixed-bed stainless-steel tubular microreactor (d_{int} = 8 mm) operating under atmospheric pressure at 493 K with a H_2/CO molar ratio of 2. The catalyst was crushed and sieved to obtain catalyst grains 63–200 μm in diameter. The catalyst loading was typically 0.5 g. Before reaction, the samples were reduced in hydrogen flow at 673 K for 5 h. The thermocouple was in direct contact with the catalyst, so that the thermocouple measurements could reflect the temperature inside the reactor. No temperature spike and temperature swings were observed during the whole catalytic testing at atmospheric pressure. The temperature ramp procedure used in this paper during the startup procedure was as follows: from 323 K to 423 K, 3 K/min, then from 423 K to 493 K, 1 K/min.

Carbon monoxide contained 5% N_2, which was used as an internal standard. Analysis of H_2, CO, CO_2 and CH_4 was performed with a 13X molecular-sieve column, while hydrocarbons (C1–C20) were separated in 10% CP-Sil5 on a Chromosorb WHP packed column. The selectivity of hydrocarbons was calculated on carbon basis. The FT reaction rate is expressed as a cobalt-time yield (in moles of converted CO per second divided by the total amount of cobalt (in moles) loaded into the reactor).

3. Results

3.1. Cobalt precursor decomposition

Cobalt and ruthenium precursors in the impregnated and dried silica-supported catalysts were decomposed either by calcination or by glow discharge plasma. The catalyst calcination temperature was chosen on the basis of TGA data. The TGA curves of bulk cobalt nitrate and monometallic impregnated and dried Co/SiO_2 catalyst in air flow are shown in Fig. 2. Two weight losses were observed at around 361 K (∼11.7%) and 459 K (∼13.8%) during the heating of Co/SiO_2 sample (Fig. 2a), which were attributed respectively to the dehydration of cobalt nitrate and silica and to the decomposition of NO_3^- groups. In agreement with previous results [32], a more complex curve was displayed in the process of decomposition of bulk cobalt nitrate (Fig. 2b), several weight change peaks appeared during heating, which might be due to the dehydration and decomposition of cobalt nitrate from the surface to the core. The complete decomposition temperature of bulk cobalt nitrate

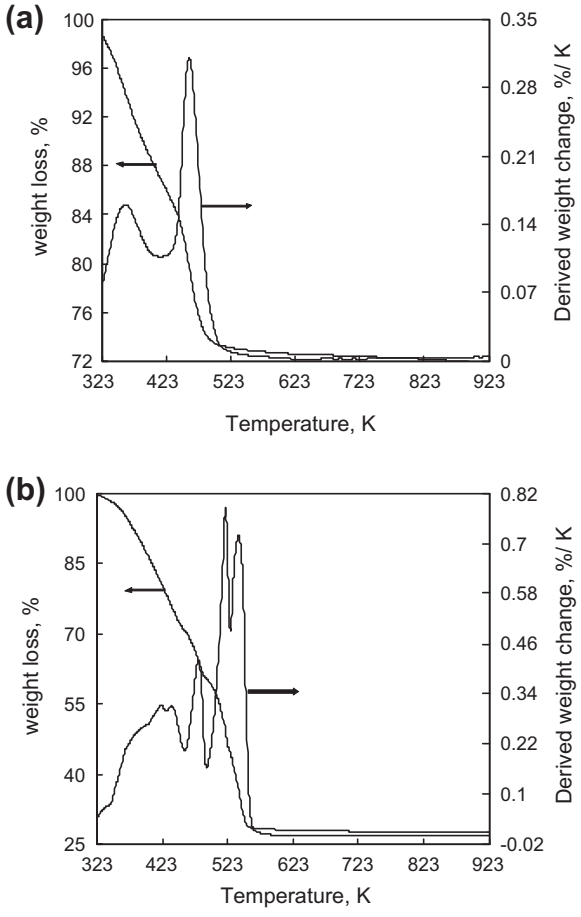

Fig. 2. TGA curves of dried Co/SiO_2 sample (a) and bulk cobalt nitrate (b). Temperature ramp 5 K/min.

(~573 K) is much higher than that of supported Co/SiO_2 catalyst (~513 K). The calcination temperature of 523 K seems sufficient to ensure complete thermal decomposition of cobalt nitrate in silica-supported cobalt catalysts. Higher calcination temperature could result in the formation of hardly reducible cobalt silicates [32,33] and would affect the catalytic performance in FT synthesis. Thus, in this work, both impregnated and dried cobalt monometallic and Ru-promoted catalysts were calcined at 523 K.

During the glow discharge pretreatment, the catalysts were exposed to the plasma in the setup shown in Fig. 1. The catalyst color started changing from pink to gray in the first 5 min of plasma pretreatment. All the catalyst particles turned to black after discharging for 25 min. Catalyst color change seems to be a sign of cobalt nitrate decomposition in the plasma. The discharge voltage varied from 60 to 120 V. Plasma pretreatment led to some heating of the quartz tube. After 2 h of plasma pretreatment, the tube temperature was however still below 373 K. To enhance the catalyst stability, the samples after plasma pretreatment were calcined in air flow at 523 K using the conventional calcination procedure.

3.2. Oxidized catalysts

The XRD patterns of oxidized conventionally calcined and plasma-assisted Co and CoRu catalysts are presented in Fig. 3. All the oxidized catalysts exhibited the presence of Co_3O_4 as the only cobalt crystalline phase. The diameters of Co_3O_4 crystallites which were calculated from the width of diffraction peak at $2\theta = 59.58°$ using the Sherrer equation [26] are presented in Table 1. The Co_3O_4 crystallite diameters of plasma-assisted catalysts were smaller than those of conventionally calcined samples. In addition, the size of Co_3O_4 crystallites decreased with plasma intensity (Table 1).

The oxidized catalysts were analyzed by X-ray absorption spectroscopy at cobalt K absorption edge. The XANES spectra and EXAFS Fourier transform moduli of both oxidized monometallic and ruthenium-promoted silica-supported cobalt catalysts were similar to those of Co_3O_4 reference compound (Fig. 4). In agreement with XRD data, this suggests that Co_3O_4 is the major cobalt phase in both conventionally calcined and plasma-assisted catalysts. For a more quantitative analysis, the XANES spectra (Fig. 4a) were fitted using a linear combination of XANES spectra of reference compounds. The experimental data matched well with the linear combination fitting curves; a representative example of the fitting is shown in Fig. 5. Quality of the analysis was also evaluated by the reduced chi-square value (χ^2_V), which estimates the fit statistical goodness. The XANES data (Table 2) were indicative of the presence of both Co_3O_4 and α-cobalt silicate, while no residual cobalt nitrate was detected. Thus, the XANES analysis suggests that decomposition of cobalt nitrate in both conventional and plasma-assisted cobalt catalysts was complete after calcination at 523 K for 5 h. Co_3O_4 content was higher than 85% in both conventional and plasma-assisted samples; α-Co_2SiO_4 content was around 10% (Table 2). No noticeable effect of plasma intensity on the fraction of cobalt silicate in the oxidized catalysts was observed.

3.3. Reduction of cobalt catalysts

The influence of pretreatment with plasma on the reducibility of the silica-supported cobalt catalysts was studied by temperature-programmed reduction (TPR), *in situ* magnetic measurements and *in situ* X-ray absorption spectroscopy. Fig. 6 displays TPR profiles of silica-supported monometallic and ruthenium-promoted cobalt catalysts. The occurrence of multiple reduction peaks indicates the presence of a number of reducible cobalt oxide species and several cobalt reduction steps. Co_3O_4 is the major phase in the oxidized catalysts identified by XRD and X-ray absorption. In agreement

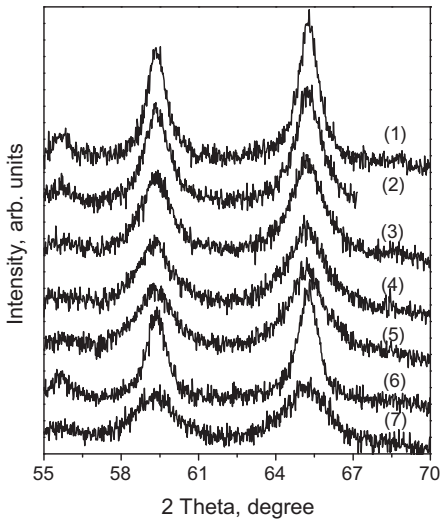

Fig. 3. XRD diffraction patterns of conventional and plasma-assisted cobalt catalysts: (1) Co/SiO_2, (2) Co/SiO_2-P60, (3) Co/SiO_2-P80, (4) Co/SiO_2-P100, (5) Co/SiO_2-P120, (6) $CoRu/SiO_2$, and (7) $CoRu/SiO_2$-P60.

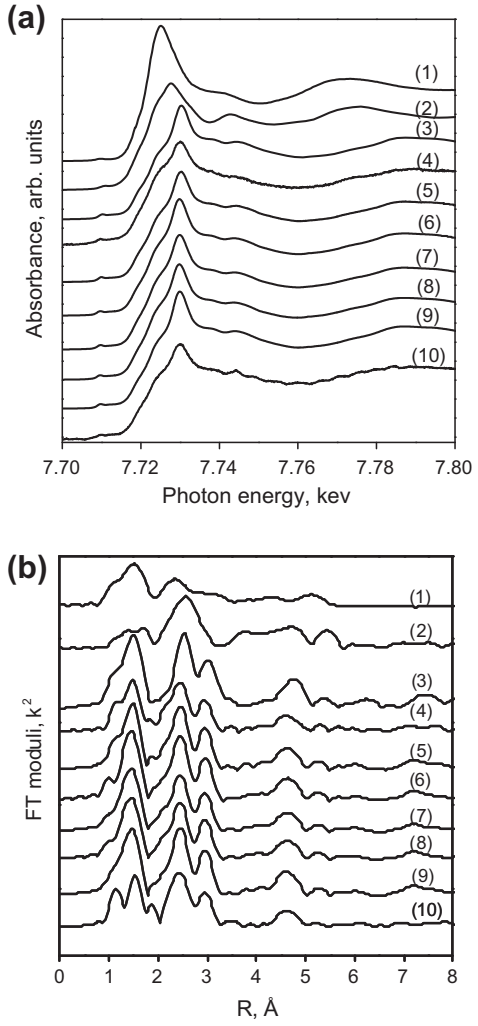

Fig. 4. XANES spectra (a) and k^2-weighted EXAFS Fourier transform moduli (b) for oxidized conventional and plasma-assisted silica-supported cobalt catalysts: (1) α-cobalt silicate, (2) CoO, (3) Co_3O_4, (4) Co/SiO_2, (5) Co/SiO_2-P60, (6) Co/SiO_2-P80, (7) Co/SiO_2-P100, (8) Co/SiO_2-P120, (9) $CoRu/SiO_2$, and (10) $CoRu/SiO_2$-P60.

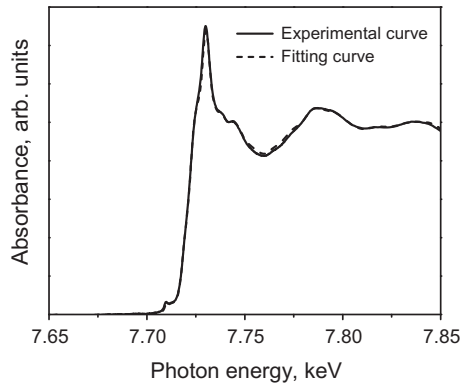

Fig. 5. XANES fitting results for Co/SiO_2 catalyst using a linear combination of XANES spectra of reference compounds: range 7.70–7.80 keV.

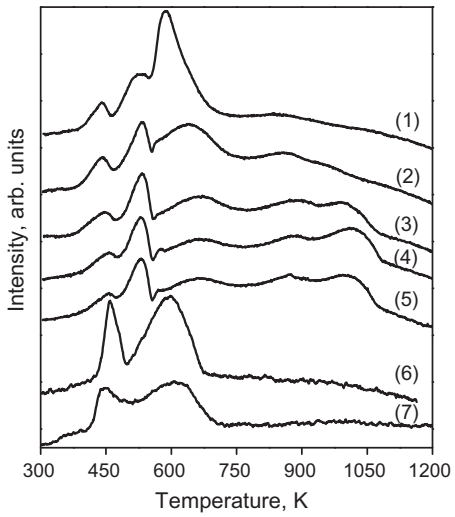

Fig. 6. TPR patterns of conventional and plasma-assisted silica-supported cobalt catalysts: (1) Co/SiO_2, (2) Co/SiO_2-P60, (3) Co/SiO_2-P80, (4) Co/SiO_2-P100, (5) Co/SiO_2-P120, (6) $CoRu/SiO_2$, and (7) $CoRu/SiO_2$-P60.

with previous reports [4,5,34–36], the TPR peaks at 373–923 K were attributed to two-step reduction of Co_3O_4, which proceeds via intermediate formation of CoO: $Co_3O_4 \rightarrow CoO \rightarrow Co^0$. The broad peaks located higher than 923 K were assigned to the reduction of cobalt oxide species, in interaction with the support (small cobalt oxide crystallites, cobalt silicates). The TPR profiles of the catalysts were significantly affected by the intensity of plasma pretreatment. The area of lower temperature peaks situated between 553 K and 723 K which corresponded to easy reducible cobalt species decreased with increasing plasma intensity, while the area of the high temperature peaks attributed to more difficult to reduce cobalt species increased. This seems to be indicative of a more difficult reduction of the plasma-assisted catalysts, particularly when high plasma intensity has been applied. Characterization of oxidized catalysts by XRD revealed the presence of smaller cobalt particles in the plasma-assisted catalysts, while no noticeable increase in the concentration of cobalt silicate was detected from XANES data (Table 2). It is known [4,34] that in silica-supported catalysts smaller cobalt oxide particles are more difficult to reduce than larger ones. Hence, the shift of TPR peaks to higher temperatures can be attributed to a higher fraction of more hardly reducible smaller cobalt oxide particles in the plasma-assisted catalysts.

In the TPR profiles of ruthenium-promoted samples, only two reduction peaks located between 400 K and 673 K were observed. These peaks were attributed to the two-step reduction of Co_3O_4. The low temperature shift of the TPR peaks of Ru-promoted catalysts relative to the monometallic counterparts (Fig. 6) indicates considerable enhancement of cobalt reducibility on promotion with ruthenium. In the plasma-assisted $CoRu/SiO_2$-P60, the area of both reduction peaks was however lower than in the conventionally calcined $CoRu/SiO_2$ catalyst, which may suggest some decrease in the extent of cobalt reduction brought about by the plasma pretreatment.

The *in situ* magnetization curves for conventionally calcined Co/SiO_2 catalysts and their plasma-assisted counterparts measured

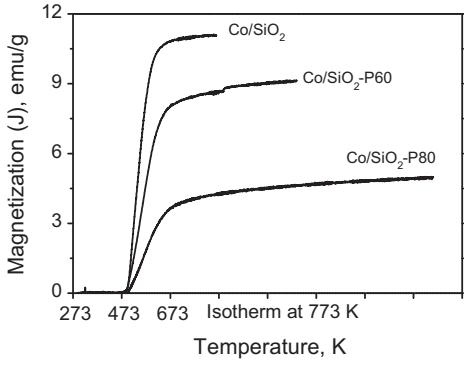

Fig. 7. *In situ* magnetization measurements of conventional and plasma-assisted monometallic catalysts during the reduction in pure hydrogen.

during reduction in hydrogen are shown in Fig. 7. Note that only metallic cobalt particles exhibit noticeable magnetization under the experimental conditions [27,37]. Thus, the increase in magnetization measured at strong magnetic field (saturation magnetization) directly indicates the growth of cobalt metallic phases in the catalysts [27,37]. Fig. 7 shows that plasma pretreatment results in a significant decrease in the magnetization of the reduced catalysts, which corresponds to lower concentrations of metallic cobalt phases. This was consistent with the observation from TPR experiments and our previous data about plasma-assisted alumina-supported cobalt catalysts [25]. Plasma of higher intensity seems to

Table 2
Cobalt phase compositions in oxidized and reduced catalysts evaluated from linear combination of XANES spectra.

Catalysts	Composition of oxidized samples			Composition of reduced samples			
	Co_3O_4 (%)	Co_2SiO_4 (%)	Reduced chi-square	Co (%)	CoO (%)	Co_2SiO_4 (%)	Reduced chi-square
Co/SiO_2	87.4	12.6	0.00019	32.8	38.6	28.6	0.00056
Co/SiO_2-P60	98.4	1.6	0.00055	7.2	56.8	36.0	0.00105
Co/SiO_2-P80	92.5	7.5	0.00036	–	–	–	
Co/SiO_2-P100	90.3	9.7	0.00020	–	–	–	
Co/SiO_2-P120	89.1	10.9	0.00032	–	–	–	
$CoRu/SiO_2$	96.9	3.1	0.00031	94.1	0	5.9	0.00131
$CoRu/SiO_2$-P60	93.6	6.4	0.00097	46.0	26.5	27.5	0.00135

affect catalyst reducibility to a much greater extent than low-intensity plasma; the saturation magnetization was 10.8 emu/g for Co/SiO_2, 8 emu/g for Co/SiO_2-P60 and only 3.6 emu/g for Co/SiO_2-P80.

The TPR data and *in situ* magnetic results on cobalt reducibility were consistent with *in situ* XANES and EXAFS findings. Fig. 8 shows *in situ* XANES spectra and EXAFS Fourier transform moduli of Co/SiO_2 and $CoRu/SiO_2$ catalysts and their plasma-assisted counterparts reduced in hydrogen at 673 K. Both XANES spectra and Fourier transform moduli were different for conventionally calcined and plasma-assisted samples. Note that the differences in the XANES region could be related to the changes in both electronic properties (oxidation state) and local coordination of the absorbing atoms [38]. The extent of cobalt reduction in silica-supported cobalt catalysts seems to be a function of plasma pretreatment and promotion with ruthenium. The XANES curves (Fig. 8a) were fitted using a linear combination of XANES spectra of metallic cobalt, CoO and α-Co_2SiO_4 as reference compounds. The fitting (Table 2) showed a much higher content of CoO and a much lower fraction of metallic cobalt in the plasma-assisted cobalt catalysts compared to the conventionally calcined counterparts. Plasma pretreatment seems to affect cobalt reducibility in both monometallic and Ru-promoted catalysts. Another interesting observation is that the concentration of cobalt silicate has increased after catalyst reduction in hydrogen at 673 K relative to the oxidized samples (Table 2). This suggests that some cobalt silicate possibly forms during catalyst reduction in addition to cobalt silicate already present in the catalysts after calcination. The cobalt silicate fraction was more significant in the monometallic catalysts which are more difficult to reduce and which contain higher fraction of CoO phase than in Ru-promoted samples. At the higher reduction temperature, CoO phase can probably react with SiO_2 yielding cobalt silicate compounds:

$$2CoO + SiO_2 \rightarrow Co_2SiO_4.$$

Water produced during the reduction of cobalt oxide could also play a role in cobalt silicate formation during catalyst reduction. Fig. 9 displays *in situ* synchrotron-based XRD patterns obtained after reduction of conventionally calcined and plasma-assisted cobalt catalysts at 623 K. No XRD peaks attributed to cobalt oxide are observed; all cobalt crystalline phases (except for amorphous cobalt silicate) seem to be completely reduced. A broad region of diffraction is observed between 12.5° and 16.5° close to the position of XRD patterns of cobalt fcc and hcp metallic phases. The most intense peak which corresponds to cobalt fcc structure was detected at 14°. Similar XRD patterns for reduced silica-supported cobalt catalysts have been previously observed in the literature [4,39]. Significant broadening of XRD patterns of $CoRu/SiO_2$-P60 catalyst relative to $CoRu/SiO_2$ seems to be indicative of smaller sizes of cobalt metal particles and higher cobalt dispersion in the plasma-assisted catalysts. This is consistent with smaller sizes of cobalt oxide crystallites detected by XRD in the oxidized plasma-assisted samples (Table 1). The XRD patterns were fitted using the whole pattern matching procedure and FullProf program [40]. The fitting suggests that the treatment of $CoRu/SiO_2$ catalyst with plasma results in the decrease in sizes of cobalt metal particles with fcc lattice from 4.4 to 2.7 nm, while the size of cobalt hcp metal particles drops from 2.6 to 2.0 nm.

The number of cobalt surface metal sites in the reduced cobalt catalysts was evaluated by propene chemisorption (Table 1). The catalyst pretreatment with glow discharge plasma of low intensity results in a slight increase in the number of cobalt surface sites in Co/SiO_2-P60, while high intensity of glow discharge leads to a drop in the number of active sites in Co/SiO_2-P120 sample. As expected, ruthenium promotion resulted in a much higher concentration of cobalt metal sites probably because of better reducibility of $CoRu/SiO_2$ and $CoRu/SiO_2$-P60 catalysts.

3.4. Catalytic performance of silica-supported cobalt catalysts

The catalytic performance of plasma-assisted monometallic and ruthenium-promoted silica-supported cobalt catalysts was evaluated in a fixed-bed reactor at 493 K, 1 bar, $H_2/CO = 2$ and GHSV = 1800 ml/(g_{cat} h). C1–C20 hydrocarbons and water were the only reaction products; no carbon dioxide was detected under the present conditions. The FT reaction rates expressed as cobalt-time yields were calculated from carbon monoxide conversions and gas hourly space velocities and normalized by the number of cobalt atoms loaded in the reactor.

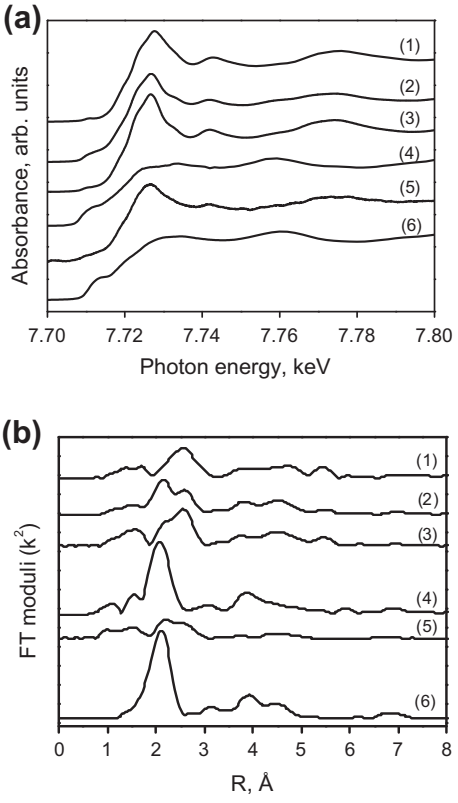

Fig. 8. *In situ* XANES spectra (a) and k^2-weighted EXAFS Fourier transform moduli (b) for (1) CoO, (2) reduced Co/SiO_2, (3) reduced Co/SiO_2-P60, (4) reduced $CoRu/SiO_2$, (5) reduced $CoRu/SiO_2$-P60 and (6) metallic cobalt.

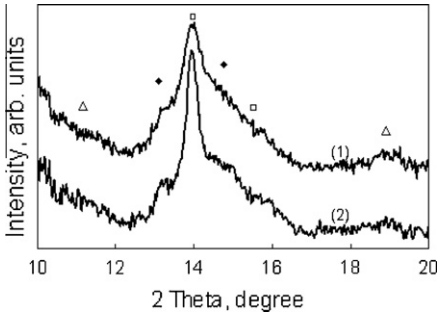

Fig. 9. *In situ* synchrotron-based XRD patterns (λ = 0.5 Å) of reduced $CoRu/SiO_2$-P60 (1) and $CoRu/SiO_2$ (2) catalysts (□ fcc metallic cobalt, ♦ hcp metallic cobalt, △ CoO). The XRD patterns were measured in a flow of hydrogen at 423 K.

Fig. 10 shows FT reaction rates, methane selectivity and C_{5+} selectivity, versus the time on stream for $CoRu/SiO_2$ sample. FT reaction rates decreased slightly and maintained around $11.5 \times 10^{-4}\ s^{-1}$ during 24 h test, and the quasi-steady state was attained after about 2 h, whereas the hydrocarbon selectivities remained at the same level. The activity and selectivity values reported here corresponded to the period of quasi-steady state behavior, which was typically attained after 24 h of reaction.

The experimental results at quasi-steady state conditions are summarized in Table 3 and Fig. 11. The Co/SiO_2-P60 catalyst prepared using low plasma intensity had a slightly higher activity than their conventional counterpart, the cobalt-time yield increased from $6.79 \times 10^{-4}\ s^{-1}$ over conventional Co/SiO_2 to $8.38 \times 10^{-4}\ s^{-1}$ over the plasma-pretreated catalyst. Further increasing plasma intensity caused a decrease in the catalytic activity, the FT reaction rate dropped from $8.38 \times 10^{-4}\ s^{-1}$ at voltage of 60 V to $4.46 \times 10^{-4}\ s^{-1}$ at voltage of 120 V. Both conventional and plasma-assisted monometallic cobalt catalysts were much less active in FT synthesis than ruthenium-promoted cobalt catalysts. The plasma-assisted $CoRu/SiO_2$-P60 catalyst exhibited a cobalt-time yield of $14.70 \times 10^{-4}\ s^{-1}$, which was higher than that obtained with conventional ruthenium-promoted catalyst ($11.90 \times 10^{-4}\ s^{-1}$). The selectivity to C_{5+} hydrocarbons and methane of both conventional and plasma-assisted Co and CoRu catalysts did not vary much as a function of plasma pretreatment and ruthenium promotion (Table 3).

4. Discussion

High cobalt dispersion along with adequate cobalt reducibility seems to be key parameters in the design of active catalysts for FT synthesis. Cobalt dispersion in FT catalysts can be enhanced by several different techniques: optimization of support texture [12,41–43], decomposition of cobalt precursors and catalyst calcination at mild conditions [32,44–46] or in the presence of NO/He [47,48], addition of organic compounds during impregnation [30,49–53] and catalyst promotion [30,54,55]. The results obtained in this work suggest that decomposition of cobalt precursors in glow discharge plasma seems to be another valuable method which can be used for preparation of highly dispersed cobalt catalysts. Higher cobalt dispersion was observed in both oxidized and reduced plasma-assisted Co/SiO_2 catalysts. It appears that glow discharge plasma pretreatment results in the decomposition of cobalt nitrate and in the formation of cobalt oxide nanoparticles which are smaller than those typically obtained after decomposition of cobalt nitrate via conventional calcination. Oxidized plasma-assisted samples also contain some concentration of cobalt silicate. Interestingly, the concentration of cobalt silicate is not affected by the intensity of plasma pretreatment, while higher plasma intensity leads to smaller sizes of cobalt oxide crystallites.

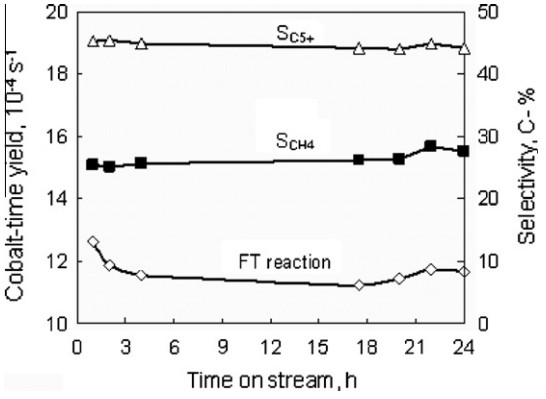

Fig. 10. FT reaction rates, methane and C_{5+} selectivities as functions of time on stream on $CoRu/SiO_2$ sample. (Conditions: $P = 1$ bar, $T = 493$ K, GHSV = 1800 ml/(g h)$^{-1}$, $H_2/CO = 2$.)

Table 3
Catalytic performances of conventional and plasma-assisted cobalt catalysts in FT synthesis.[a]

Catalysts	CO conversion (%)	Cobalt-time yield ($10^{-4}\ s^{-1}$)	Selectivity (%)		
			CH_4	C_{2-4}-HC	C_{5+}-HC
Co/SiO_2	17.5	6.79	30.7	26.2	43.1
Co/SiO_2-P60	21.6	8.38	25.5	30.7	43.8
Co/SiO_2-P80	16.5	6.40	27.0	31.5	41.5
Co/SiO_2-P100	12.9	5.01	25.3	31.0	43.7
Co/SiO_2-P120	11.5	4.46	26.2	31.9	41.9
$CoRu/SiO_2$	30.7	11.90	27.1	28.6	44.3
$CoRu/SiO_2$-P60	38.0	14.70	24.9	30.4	44.7

[a] Conditions: $P = 1$ bar, 500 mg catalysts, $T = 493$ K, gas hourly space velocity (GHSV) = 1800 ml/(g h)$^{-1}$, $H_2/CO = 2$.

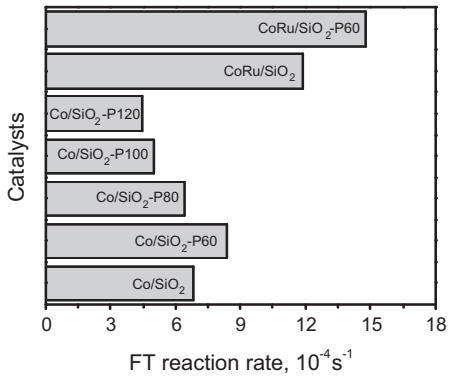

Fig. 11. FT reaction rates on conventional calcined and plasma-assisted catalysts.

Previous reports have shown [2,10,30,47] that both decomposition of cobalt nitrate and crystallization of cobalt oxide could be crucial steps in the preparation of highly dispersed cobalt catalysts. The size of cobalt oxide crystallites in the catalysts is influenced by the rates of cobalt nitrate decomposition, cobalt oxide nucleation and crystal growth. Slower rate of cobalt nitrate decomposition generally favors high cobalt dispersion. De Jong and coworkers [47,48] used NO/He mixture to decompose metal nitrate in cobalt and nickel-supported catalysts. Higher metal dispersion was attributed to a more moderate rate of metal nitrate decomposition in the presence of NO. Note that decomposition of cobalt precursors in glow discharge proceeds at much milder conditions (at much lower temperatures). Milder cobalt nitrate decomposition conditions are usually favorable for better cobalt dispersion than conventional calcination.

Crystallization of cobalt oxide involves essential stages of nucleation and crystal growth. Higher rate of crystal nucleation leads to smaller crystallite sizes, while higher rate of crystal growth favors larger crystallite sizes. The presence of relatively larger cobalt oxide crystallites in monometallic silica-supported cobalt catalysts can be explained by low rate of crystal nucleation and high rate of crystal growth. It was shown [30] that promotion of silica-supported cobalt catalysts with noble metals (Ru, Re) enhanced cobalt dispersion. This effect can be due to a higher concentration of cobalt oxide nucleation sites in the presence of promoters [30].

It appears that in addition to the mechanism of cobalt nitrate decomposition, the kinetics of cobalt oxide nucleation and crystal growth can be also affected by the plasma. Interaction of plasma

with the catalyst surface could possibly generate defects in the support structure which can facilitate formation of seed crystals and enhance the rate of cobalt oxide nucleation.

The plasma pretreatment also has influence on cobalt reducibility. TPR, *in situ* magnetic characterization and *in situ* X-ray absorption spectroscopy were indicative of a more difficult cobalt reducibility in the plasma-assisted catalysts. It seems that a decrease in cobalt oxide particle size produced by plasma pretreatment impedes cobalt reduction. This observation is consistent with previous results for silica-supported cobalt catalysts. It has been shown that smaller cobalt oxide particles are more difficult to reduce than larger ones [4,34].

It is known that the contribution of surface energy to the total energy of the cobalt oxide and cobalt metallic particles depends on their size; the part of surface energy in the total energy is more significant for smaller particles. Hence, the stability of smaller particles is to a greater extent influenced by their surface energy than that of the larger particles. van Steen et al. [56] evaluated the surface energy of cobalt oxide and cobalt metal particles as a function of their size. It was found that cobalt metal particles had higher surface energy than particles of cobalt oxide. In agreement with those data [56], a more difficult reducibility of smaller cobalt particles can be attributed to the higher surface energy of cobalt metal phases.

In addition, the stability of cobalt particles can be affected by the support. A weak interaction of metal and support is a particularity of silica-supported catalysts. In the conventionally calcined silica-supported catalysts, relatively large cobalt oxide particles are present. These large cobalt oxide particles can be relatively easily reduced to metallic cobalt in hydrogen. When cobalt oxide particles are forced to be small by using glow discharge plasma, decomposition of cobalt precursor in NO, narrow pore catalytic support or any other methods, this would necessarily cause a more surface interaction between cobalt oxide and silica. Thus, cobalt reducibility becomes an issue. Consequently, a more difficult reducibility of smaller cobalt oxide particles in the plasma-assisted catalysts would shrink the number of active sites. This effect was observed using propene chemisorption in the Co/SiO_2-P120 catalysts which has lesser cobalt metal sites than the conventionally calcined Co/SiO_2 counterpart (Table 1).

In agreement with previous reports [2,3,13,57–60], cobalt reducibility can be improved by promotion with noble metals (e.g. ruthenium). Indeed, a higher fraction of cobalt metallic phases was observed by *in situ* X-ray absorption in the reduced Ru-promoted catalysts relative to the monometallic counterparts (Table 2). Very low concentration of cobalt species reducible at temperature higher than 773 K was detected by TPR in CoRu catalysts (Fig. 6). *In situ* XRD was indicative of higher cobalt dispersion in the reduced Ru-promoted cobalt catalysts pretreated with glow discharge plasma (Fig. 9).

It is known [1,2,7,8,11] that FT synthesis occurs on the cobalt metal sites, which is situated on the surface of cobalt metal particles. The number of surface cobalt metal sites is a function of both cobalt reducibility and cobalt dispersion. Hence, the catalyst, which combines high cobalt dispersion with good cobalt reducibility, would have a large number of active cobalt metal sites, and thus, a better FT catalytic performance. Our results show that plasma pretreatment of silica-supported cobalt catalysts leads to smaller cobalt particles than conventional calcination, but at the same time hinders to some extent cobalt reducibility. This is consistent with the experimentally observed variation of FT reaction rates as a function of plasma intensity. Indeed, cobalt-time yield first slightly increased from $6.79 \times 10^{-4}\ s^{-1}$ on Co/SiO_2 to $8.38 \times 10^{-4}\ s^{-1}$ on Co/SiO_2-P60 when plasma of lower intensity was used for catalyst pretreatment, but then dropped to $4.46 \times 10^{-4}\ s^{-1}$ on Co/SiO_2-P120, when plasma of higher intensity was involved.

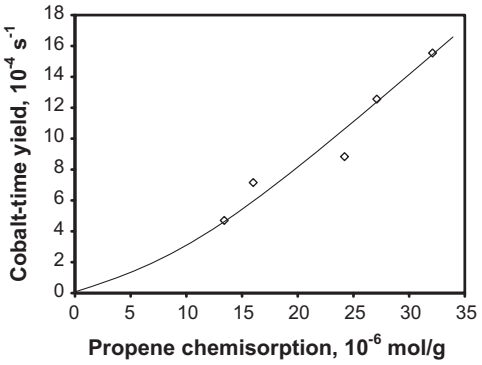

Fig. 12. Cobalt-time yield on conventional calcined and plasma-pretreated catalysts as a function of propene chemisorption.

The dependence of cobalt-time yields on propene chemisorption for conventionally calcined and plasma-assisted silica-supported cobalt catalysts is shown in Fig. 12. In agreement with previous results [3,30,31], the catalysts with high number of cobalt metal sites display higher FT reaction rates. An attempt was made to estimate the FT turnover frequencies on silica-supported cobalt catalysts using propene chemisorption data. Note that propene chemisorption does not provide information about the absolute number of cobalt surface in the catalyst, only relative amounts can be measured [31]. FT reaction rates calculated from carbon monoxide conversions, gas hourly space velocities and normalized by propene chemisorption instead of overall cobalt contents were nearly constant for the conventionally calcined and plasma-assisted catalysts ($\sim 6–8 \times 10^{-2}\ s^{-1}$). This finding is also consistent with quasi-linearity of the dependence between cobalt-time yield and propene chemisorption displayed in Fig. 12. Thus, the silica-supported catalysts studied in this work exhibit very week dependence of FT turnover frequency on cobalt particle size.

Higher FT reaction rates were observed on the Ru-promoted catalysts. It appears that much higher FT reaction rates exhibited in these catalysts are due to a better cobalt reducibility. The effect was more pronounced with plasma-assisted $CoRu/SiO_2$-P60 catalysts which had both higher cobalt dispersion and good cobalt reducibility. Thus, an enhancement of cobalt dispersion by glow discharge plasma in concert with the promotion with ruthenium, which preserves cobalt reducibility, seems to be a potential approach to improve the catalytic performance of cobalt catalysts in FT synthesis.

5. Conclusion

It was found that pretreatment of impregnated and dried silica-supported monometallic and ruthenium-promoted cobalt catalysts with glow discharge plasma yielded smaller cobalt particles than conventional calcination. Cobalt dispersion was influenced primarily by the plasma intensity; higher plasma intensity led to higher cobalt dispersion. The concentration of cobalt silicate in plasma-assisted samples was low. Smaller cobalt particles in the plasma-assisted monometallic cobalt catalysts displayed more difficult cobalt reduction than larger cobalt particles in the conventionally calcined counterparts. Slightly lower activity of plasma-assisted monometallic cobalt catalysts was attributed to lower cobalt reducibility. Promotion with ruthenium resulted in a significant increase in cobalt reducibility in both plasma-assisted and conventionally calcined catalysts. Due to the combination of high cobalt dispersion and good cobalt reducibility, Ru-promoted plasma-assisted cobalt catalysts exhibited enhanced FT reaction rate. Glow discharge plasma seems to be an important tool which can be used

to enhance cobalt dispersion and to improve catalytic performance of cobalt FT catalysts.

Acknowledgments

J.H. thanks the Embassy of France in China for a Ph.D. Fellowship. The supports from the Natural Science Foundation of China (NSFC 205903603) and the 985 Project and 211 Project of Sichuan University are also acknowledged. The authors thank L. Burylo, O. Gardoll, L. Olivi, A. Cognigni and O. Safonova for the help with conventional X-ray diffraction, TPR measurements and synchrotron experiments respectively. The authors would like to thank Prof. E. Payen, Prof. X.Y. Dai, the colleagues in the Unité de catalyse et de chimie du solide, UMR CNRS 8181 of France and those of 230 Lab of Sichuan University for useful discussions. The Elettra Synchrotron Light Laboratory (BL11.1 beamline) and European Synchrotron Radiation Facility (SNBL beam line) are acknowledged for the use of synchrotron radiation.

References

[1] M.E. Dry, Catal. Today 71 (2002) 227.
[2] A.Y. Khodakov, W. Chu, P. Fongarland, Chem. Rev. 107 (2007) 1692.
[3] A.Y. Khodakov, Catal. Today 144 (2009) 251.
[4] A.Y. Khodakov, J. Lynch, D. Bazin, B. Rebours, N. Zanier, B. Moisson, P. Chaumette, J. Catal. 168 (1997) 16.
[5] R. Bechara, D. Balloy, J.-Y. Dauphin, J. Grimblot, Chem. Mater. 11 (1999) 1703.
[6] A. Martínez, G. Prieto, J. Catal. 245 (2007) 470.
[7] E. Iglesia, Appl. Catal. A 161 (1997) 59.
[8] Ø. Borg, P.D.C. Dietzel, A.I. Spjelkavik, E.Z. Tveten, J.C. Walmsley, S. Diplas, S. Eri, A. Holmen, E. Rytter, J. Catal. 259 (2008) 161.
[9] S.L. Soled, E. Iglesia, R.A. Fiato, J.E. Baumgartner, H. Vroman, S. Miseo, Top. Catal. 26 (2003) 101.
[10] J. van de Loosdrecht, S. Barradas, E.A. Caticato, N.G. Ngwenya, P.S. Nkwanyana, M.A.S. Rawat, B.H. Sigwebela, P.J. van Berge, J.L. visagie, Top. Catal. 26 (2003) 121.
[11] G.L. Bezemer, J.H. Bitter, H.P.C.E. Kuipers, H. Oosterbeek, J.E. Holewijn, X. Xu, F. Kapteijn, A. Jos van Dillen, K.P. de Jong, J. Am. Chem. Soc. 128 (2006) 3956.
[12] A.Y. Khodakov, A. Griboval-Constant, R. Bechara, V.L. Zholobenko, J. Catal. 206 (2002) 230.
[13] W. Chu, P.A. Chernavskii, L. Gengembre, G.V. Pankina, P. Fongarland, A.Y. Khodakov, J. Catal. 252 (2007) 215.
[14] P.B. Radstake, J.P.D. Breejen, G.L. Bezemer, J.H. Bitter, K.P.D. Jong, V. Frøseth, A. Holmen, Stud. Surf. Sci. Catal. 167 (2007) 85.
[15] C. Liu, G.P. Vissokov, B.W.L. Jang, Catal. Today 72 (2002) 173.
[16] J.J. Zou, C.J. Liu, Y.P. Zhang, Langmuir 22 (2006) 2334.
[17] C. Liu, K. Yu, Y. Zhang, X. Zhu, F. He, B. Eliasson, Catal. Commun. 4 (2003) 303.
[18] G. Liu, W. Chu, H. Long, X. Dai, Y. Yin, Chin. J. Catal. 28 (2007) 582.
[19] C. Liu, K. Yu, Y. Zhang, X. Zhu, F. He, B. Eliasson, Appl. Catal. B 47 (2004) 95.
[20] J.G. Wang, C.J. Liu, Y.P. Zhang, K.L. Yu, X.L. Zhu, F.E.I. He, Catal. Today 89 (2004) 183.
[21] Y. Zhang, P. Ma, X. Zhu, C. Liu, Y. Shen, Catal. Commun. 5 (2004) 35.
[22] J.-J. Zou, C. Chen, C.-J. Liu, Y.-P. Zhang, Y. Han, L. Cui, Mater. Lett. 59 (2005) 3437.
[23] M.H. Chen, W. Chu, X.Y. Dai, X.W. Zhang, Catal. Today 89 (2004) 201.
[24] Y. Zhang, W. Chu, W. Cao, C. Luo, X. Wen, K. Zhou, Plasma Chem. Plasma Process 20 (2000) 137.
[25] W. Chu, L. Wang, P.A. Chernavskii, A.Y. Khodakov, Angew. Chem. Int. Ed. 47 (2008) 5052.
[26] B.D. Cullity, Elements of X-ray Diffraction, Addison-Wesley Publishing Company, London, 1978.
[27] V.V. Kiselev, P.A. Chernavskii, V.V. Lunin, Russ. J. Phys. Chem. 61 (1987) 151.
[28] P.A. Chernavskii, A.Y. Khodakov, G.V. Pankina, J.-S. Girardon, E. Quinet, Appl. Catal. A 306 (2006) 108.
[29] J.-S. Girardon, A.Y. Khodakov, M. Capron, S. Cristol, C. Dujardin, F. Dhainaut, S. Nikitenko, F. Meneau, W. Bras, E. Payen, J. Synchrotron Radiat. 12 (2005) 680.
[30] J.-S. Girardon, E. Quinet, A. Griboval-Constant, P.A. Chernavskii, L. Gengembre, A.Y. Khodakov, J. Catal. 248 (2007) 143.
[31] A.S. Lermontov, J.-S. Girardon, A. Griboval-Constant, S. Pietrzyk, A.Y. Khodakov, Catal. Lett. 101 (2005) 117.
[32] J.-S. Girardon, A.S. Lermontov, L. Gengembre, P.A. Chernavskii, A. Griboval-Constant, A.Y. Khodakov, J. Catal. 230 (2005) 339.
[33] J.M. Jabłoński, M. Wocyrz, L. Krajczyk, J. Catal. 173 (1998) 530.
[34] D.G. Castner, P.R. Watson, I.Y. Chan, J. Phys. Chem. 94 (1990) 819.
[35] B. Ernst, A. Bensaddik, L. Hilaire, P. Chaumette, A. Kiennemann, Catal. Today 39 (1998) 329.
[36] A.Y. Khodakov, A. Griboval-Constant, R. Bechara, F. Villain, J. Phys. Chem. B 105 (2001) 9805.
[37] P.A. Chernavskii, J.-A. Dalmon, N.S. Perov, A.Y. Khodakov, Oil Gas Sci. Technol. 64 (2009) 25.
[38] D. Koningsberger, R. Prins, X-ray Absorption: Principles, Applications Techniques of EXAFS, SEXAFS and XANES, Wiley-Interscience, New York, 1988.
[39] O. Ducreux, B. Rebours, J. Lynch, M. Roy-Auberger, D. Bazin, Oil Gas Sci. Technol. 64 (2009) 49.
[40] J. Rodriguez-Carvajal, Physica B 192 (1993) 55.
[41] A.Y. Khodakov, R. Bechara, A. Griboval-Constant, Stud. Surf. Sci. Catal. 142B (2002) 1133.
[42] A.Y. Khodakov, R. Bechara, A. Griboval-Constant, Appl. Catal. A 254 (2003) 273.
[43] A. Griboval-Constant, A.Y. Khodakov, R. Bechara, V.L. Zholobenko, Stud. Surf. Sci. Catal. 144 (2002) 609.
[44] J.-S. Girardon, A. Constant-Griboval, L. Gengembre, P.A. Chernavskii, A.Y. Khodakov, Catal. Today 106 (2005) 161.
[45] Ø. Borg, E.A. Blekkan, S. Eri, D. Akporiaye, B. Vigerust, E. Rytter, A. Holmen, Top. Catal. 45 (2007) 39.
[46] A.Y. Khodakov, Braz. J. Phys. 39 (2009) 171.
[47] J.R.A. Sietsma, J.D. Meeldijk, J.P. den Breejen, M. Versluijs-Helder, A.J. van Dillen, P.E. de Jongh, K.P. de Jong, Angew. Chem. Int. Ed. 46 (2007) 4547.
[48] J. R.A. Sietsma, H. Friedrich, A. Broersma, M. Versluijs-Helder, A.J. van Dillen, P.E. de Jongh, K.P. de Jong, J. Catal. 260 (2008) 227.
[49] N. Koizumi, T. Mochizuki, M. Yamada, Catal. Today 141 (2009) 34.
[50] T. Mochizuk, D. Hongo, T. Satoh, N. Koizumi, M. Yamada, Catal. Lett. 121 (2008) 52.
[51] C.C. Culross, US Patent 5, 1999, pp. 928–983.
[52] C.H. Mauldin, US Patent 5 968 991, 1999.
[53] C.H. Mauldin, US Patent 6 331 575, 2001.
[54] D. Schanke, S. Vada, E.A. Blekkan, A.M. Hilmen, A. Hoff, A. Holmen, J. Catal. 156 (1995) 85.
[55] G. Jacobs, T.K. Das, Y. Zhang, J. Li, G. Racoillet, B.H. Davis, Appl. Catal. A 233 (2002) 263.
[56] E. van Steen, M. Claeys, M.E. Dry, J. van de Loosdrecht, E.L. Viljoen, J.L. Visagie, J. Phys. Chem. B 109 (2005) 3575.
[57] F. Diehl, A.Y. Khodakov, Oil Gas Sci. Technol. 64 (2009) 11.
[58] K. Takeuchi, T. Matsuzaki, H. Arakawa, T. Hanaoka, Y. Sugi, Appl. Catal. 48 (1989) 149.
[59] H.F.J. van't Blik, D.C. Koningsberger, R. Prins, J. Catal. 97 (1986) 210.
[60] M. Reinikainen, M.K. Niemelä, N. Kakuta, S. Suhonen, Appl. Catal. A 174 (1998) 61.